Journal of Applied Electrochemistry (2005) 35:151–156
DOI 10.1007/s10800-004-6197-5

Synthesis and electrochemical properties of layered $LiNi_{1/2}Mn_{1/2}O_2$ prepared by coprecipitation

Y.-K. SUN [1]*, Y.C. BAE[1] and S.-T. MYUNG[2]
[1]*Department of Chemical Engineering, Center for Information and Communication Materials, Hanyang University, Seoul 133-791, Republic of Korea*
[2]*VK Corporation, 67 Jije-Dong, Pyongtaek-City, Kyonggi-Do 450-090, Republic of Korea*
*(*author for correspondence, e-mail: yksun@hanyang.ac.kr)*

Received 14 June 2004; accepted in revised form 18 September 2004

Key words: $Al(OH)_3$-coating, cathode materials, coprecipitation, layered structure

Abstract

Spherical $LiNi_{1/2}Mn_{1/2}O_2$ powders were synthesized from $LiOH \cdot H_2O$ and coprecipitated metal hydroxide, $(Ni_{1/2}Mn_{1/2})(OH)_2$. The average particle size of the powders was about 10 μm and the size distribution was quite narrow due to the homogeneity of the metal hydroxide, $(Ni_{1/2}Mn_{1/2})(OH)_2$. The tap-density of the $LiNi_{1/2}Mn_{1/2}O_2$ powders was approximately 2.2 g cm^{-3}, which is comparable to the tap-density of commercial $LiCoO_2$. The $LiNi_{1/2}Mn_{1/2}O_2$ electrode delivered a discharge capacity of 152, 163, 183, and 189 mA h g^{-1} in the voltage ranges of 2.8–4.3, 2.8–4.4, 2.8–4.5, and 2.8–4.6 V, respectively, with good cyclability. Furthermore, $Al(OH)_3$-coated $LiNi_{1/2}Mn_{1/2}O_2$ exhibited excellent cycling behavior and rate capability compared to the pristine electrode.

1. Introduction

Over the past 10 years, intensive research has been conducted in order to find new cathode materials to replace $LiCoO_2$ in lithium-ion batteries. Recent research has focused on layer-structured $LiNi_{1/2}Mn_{1/2}O_2$ materials as a cathode material because of its charge/discharge voltage, capacity, cyclability, thermal stability, and material cost [1–9]. The oxidation states of Ni and Mn in $LiNi_{1/2}Mn_{1/2}O_2$ in the transition metal layer are 2+ and 4+, respectively. When Li^+ is deintercalated from the host, Ni^{2+} is oxidized to Ni^{4+}, while Mn^{4+} retains its initial oxidation state [4]. It is believed that the structural stability of $LiNi_{1/2}Mn_{1/2}O_2$ is ascribed to the Mn^{4+} in host structure upon charging/discharging process.

The energy density of lithium ion batteries is related to the tap density and capacity of the active materials. Therefore, it is very important to prepare electrode materials with both a high tap density and a high specific capacity. The tap density of the powders is significantly influenced by particle morphology, particle size, particle size distribution, and crystallinity of the synthesized powders. Synthesis of spherical powders could be an effective way to increase the tap density and safety of the powders. Recently, Dahn et al. [10] reported that larger particles having a high tap-density are less reactive at high oxidized state in respect to thermal stability. Therefore, control of particle size and morphology of the final products is critical to improvement of battery performance.

$LiNi_{1/2}Mn_{1/2}O_2$ powders are typically prepared by the mixed hydroxide method by reacting the coprecipitated double hydroxide of nickel and manganese with lithium hydroxide [4, 6, 7]. The $Ni_{1/2}Mn_{1/2}(OH)_2$ precursors are usually synthesized by batch-type precipitation, in which the precipitates are formed by dropping a transition metal precursor solution into a precipitation agent such as LiOH or NaOH. This method may induce irregular shaped particles with a wide size distribution because two different reactants are locally reacted for a short period of time resulting in a local concentration gradient at the reaction point of the two reactants. Also, the manganese ion is easily oxidized to a trivalent or tetravalent state, even with a trace amount of oxygen dissolved in the aqueous solution, leading to an insufficient solid solution formation at the atomic level. These disadvantages result in the irregular shaped particles and lower tap density of $LiNi_{1/2}Mn_{1/2}O_2$ powders.

$LiNi_{1/2}Mn_{1/2}O_2$ showed relatively poor rate capability at higher C-rates due to lower electronic conductivity compared to $LiCoO_2$ and $LiNi_{1/3}Co_{1/3}Mn_{1/3}O_2$ [8]. In order to use $LiNi_{1/2}Mn_{1/2}O_2$ in high power batteries, further improvement is necessary, especially at elevated temperature. One strategy to improve the electrochemical performance is to modify the surface properties of the cathode materials by coating the particles with metal oxide to prevent dissolution of transition metals and

unwanted reactions between the cathode and the electrolyte. It is well known that coating the surface of electrode active materials with various metal oxides such as ZnO, Al_2O_3, ZrO_2, TiO_2, and SiO_2 can greatly improve their electrochemical performance at elevated temperature [11–13].

In this study, we report on the synthesis and electrochemical performance of spherical $LiNi_{1/2}Mn_{1/2}O_2$ powders with high tap density. The effect of coating the $LiNi_{1/2}Mn_{1/2}O_2$ particle surface with $Al(OH)_3$ on rate capability and cyclability are also investigated.

2. Experimental

An aqueous solution of $NiSO_4$ and $MnSO_4$ (cationic ratio of Ni:Mn=1:1) with a concentration of 2.0 mol dm^{-3} was pumped into a specially designed continuous stirred tank reactor (CSTR) under nitrogen atmosphere. At the same time, 2.0 mol dm^{-3} of NaOH solution and 1.2 mol dm^{-3} of NH_4OH solution as a chelating agent were also separately fed into the reactor. The concentration of the solution, pH, temperature, and stirring speed of the mixture in the reactor were all carefully controlled. The solution pH was controlled by NaOH solution and maintained at pH 11.0. The stirring speed was set to 800 rpm during the precipitation process. At the initial stage of the coprecipitation reaction, irregular secondary particles from the agglomeration of the acicular primary structure were formed and irregular particles gradually changed into spherical particles after 12 h and vigorous stirring. The spherical $(Ni_{1/2}Mn_{1/2})(OH)_2$ particles were filtered and dried at 110 °C. The obtained spherical $(Ni_{1/2}Mn_{1/2})(OH)_2$ and $LiOH \cdot H_2O$ powders with a molar ratio 1:1.05 were mixed thoroughly. The excess amount of Li was used to compensate for the loss of Li during the calcinations. The mixture was heated at 480 °C for 5 h and calcined at 1000 °C for 10 h, and then slowly cooled to room temperature at a rate of 2 °C min^{-1}.

The $LiNi_{1/2}Mn_{1/2}O_2$ powder surface was coated by $Al(OH)_3$ first dissolving aluminum isoproxide, $Al(C_3H_7O)_3$, in isopropanol followed by the addition of distilled water. The synthesized $LiNi_{1/2}Mn_{1/2}O_2$ powders were poured into the solution and mixed for 4 h at 50 °C. The $Al(OH)_3$-coated $LiNi_{1/2}Mn_{1/2}O_2$ powders were filtered and dried at 110 °C. The amount of $Al(OH)_3$ in the coating solution corresponded to 1 wt.% of the $LiNi_{1/2}Mn_{1/2}O_2$ powders.

Powder X-ray diffraction (Rigaku, Rint-2000) using a CuKα radiation was used to identify the crystalline phase of the as-prepared powders. The particle morphologies of the $LiNi_{1/2}Mn_{1/2}O_2$ powders were observed using a field-emission scanning electron microscope (FE-SEM, JSM-6340F, JEOL). Charge/discharge cycles were performed in CR2032 coin type cells. The cell consisted of the cathode and the lithium metal anode separated by the porous polypropylene film. For the fabrication of the electrode, the mixture, which contained 20 mg of $LiNi_{1/2}Mn_{1/2}O_2$ powders and 5 mg conducting binder (3.3 mg of teflonized acetylene black (TAB) and 1.7 mg of graphite), was pressed on a 2.0 cm^2 stainless screen at 500 kg cm^{-2}. The electrolyte (Jaeil Chemical Co.) was ethylene carbonate:dimethyl carbonate (1:2 in volume) containing 1 M $LiPF_6$ by volume. AC impedance measurements were performed using a Zahner Elektrix IM6 impedance analyzer over the frequency range 1–10 mHz with an amplitude of 5 mVrms. Each sample was allowed to equilibrate for 10 h before the measurement.

3. Result and discussions

Figure 1 shows the X-ray diffraction patterns of the coprecipitated $(Ni_{1/2}Mn_{1/2})(OH)_2$ powders dried at 110 °C. The patterns show a turbostratic structure consisting of the intermediate phase between CdI_2-type phase and spinel phase [14]. The absence of impurity phases implies that Ni and Mn were homogeneously incorporated into the $(Ni_{1/2}Mn_{1/2})(OH)_2$ particles.

Figure 2 shows the morphology of $(Ni_{1/2}Mn_{1/2})(OH)_2$ powders and expanded views of a single particle. The hydroxide particles are composed of a large number of fine primary crystalline grains in Figure 2. Most of the particles are about 10 μm and have a narrow particle size distribution. It is well known that an aqueous ammonia solution acts as a complexing agent and controls the shape of the composite hydroxide. The alkaline solution acts as a pH adjusting agent. The pH of the mixed solution is adjusted to the proper level for coprecipiation according to the follow reactions [15]:

$$1/2Ni^{2+}(aq) + 1/2Mn^{2+}(aq) + xNH_4OH(aq) \rightarrow [Ni_{1/2}Mn_{1/2}(NH_3)_n]^{2+}(aq) + nH_2O + (x-n)NH_4OH(aq) \quad (1)$$

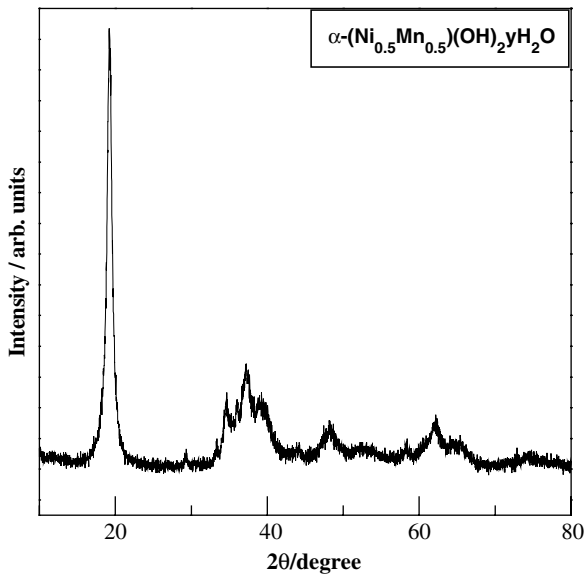

Fig. 1. Powder XRD patterns of $(Ni_{1/2}Mn_{1/2})(OH)_2$ powders.

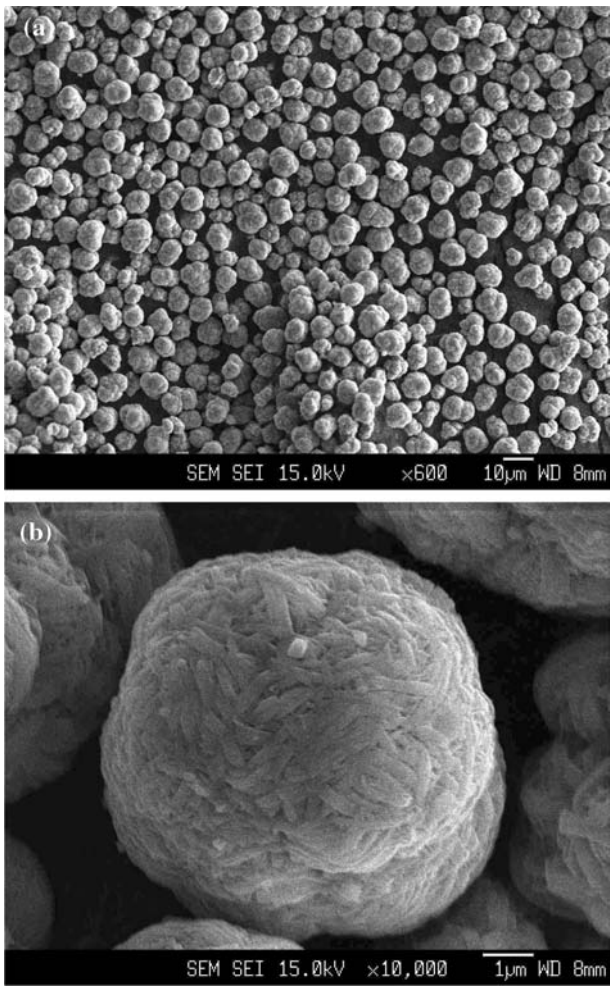

Fig. 2. SEM images of $(Ni_{1/2}Mn_{1/2})(OH)_2$ powders.

$$[Ni_{1/2}Mn_{1/2}(NH_3)_n]^{2+}(aq) + 2OH^- \rightarrow Ni_{1/2}Mn_{1/2}(OH)_2(s) + (n-2)NH_3 \quad (2)$$

The Rietveld refinement analysis of the $LiNi_{1/2}Mn_{1/2}O_2$ was shown in Figure 3. The refinement was carried out by using FULLPROF Rietveld program [16]. The refinements resulted in a very good fit between the observed and calculated patterns. The measured lattice parameters, as the hexagonal setting by the Rietveld refinements, were $a = 2.890(4)$ Å and $c = 14.296(3)$ Å, which are consistent with other reported values [3–7]. It is thought that the high homogeneity and the well-ordered layered structure of the $LiNi_{1/2}Mn_{1/2}O_2$ powders are attributable to the homogeneous spherical $Ni_{1/2}Mn_{1/2}(OH)_2$ coprecipitated precursor.

Figure 4 shows scanning electron micrographs (SEM) of the $LiNi_{1/2}Mn_{1/2}O_2$ powders. The particles have the same morphology and secondary particle size as the starting material. However, it can be seen that smaller spherical primary particles (0.1 μm in diameter in Figure 2) of the starting compound grow and become square and spherical shaped (0.5 μm). That is, the size and shape of the secondary particles hardly change during the calcination process with the primary

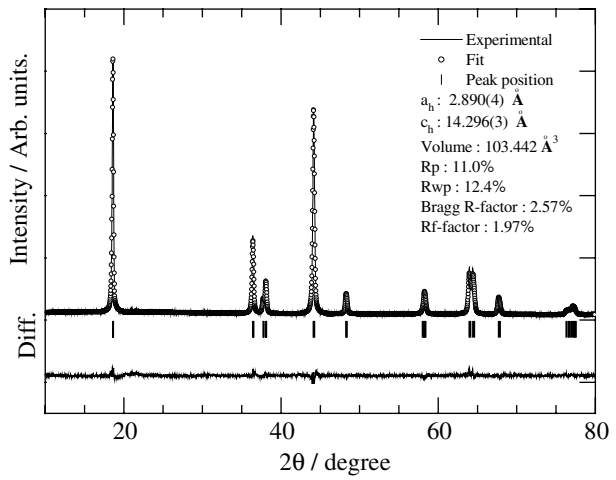

Fig. 3. Rietveld refinement XRD patterns of $LiNi_{1/2}Mn_{1/2}O_2$ powders.

structure of the particles growing slightly from 0.1 to 0.5 μm. The measured tap-density of $LiNi_{1/2}Mn_{1/2}O_2$ powders was about 2.2 g cm^{-3}. This value is close to that of commercial $LiCoO_2$.

Figure 5(a) shows the cell voltage plotted versus specific gravimetric capacity for the charge and

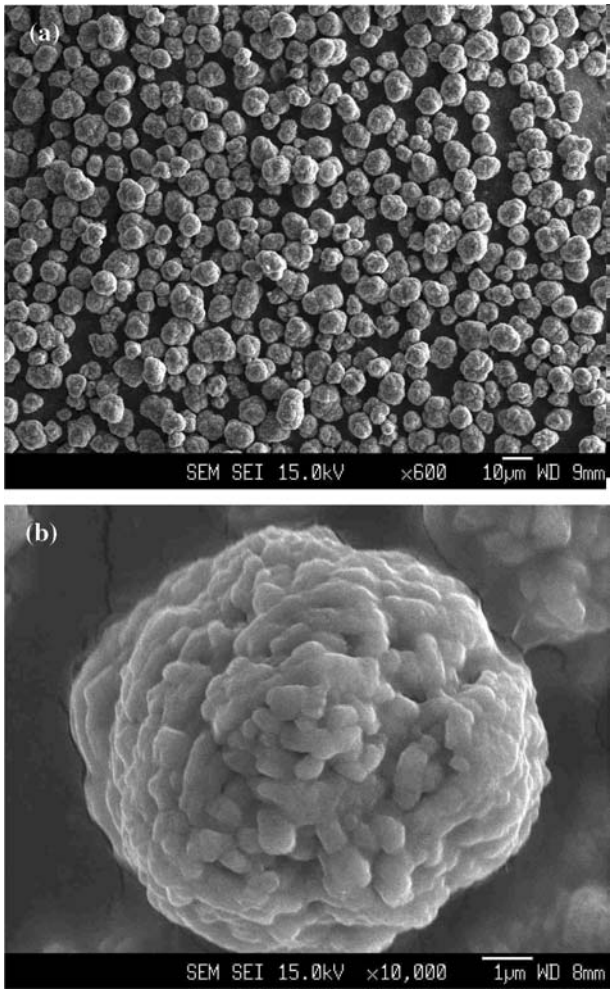

Fig. 4. SEM images of $LiNi_{1/2}Mn_{1/2}O_2$ powders.

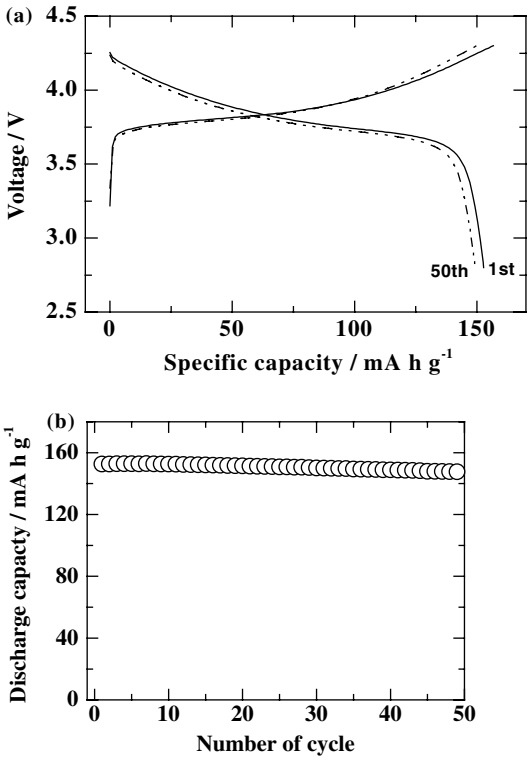

Fig. 5. (a) Cycling charge/discharge curves and (b) Variation of specific discharge capacity as a function of $Li/LiNi_{1/2}Mn_{1/2}O_2$ cell as a function of number of cycles in the voltage range of 2.8–4.3 V at a current density of 20 mA g^{-1}.

discharge of the $Li/LiNi_{1/2}Mn_{1/2}O_2$ cell at a current density of 20 mA g^{-1} between 2.8 and 4.3 V. The corresponding discharge capacities vs cycle number are shown in Figure 5(b). The $LiNi_{1/2}Mn_{1/2}O_2$ electrode has a very smooth and monotonics voltage profile and the operational voltage decays abruptly at the end of discharge, which is representative of a typical layer structured material. The $LiNi_{1/2}Mn_{1/2}O_2$ electrode exhibits excellent cycling behavior retaining 97% of its initial discharge capacity (150 mA h g^{-1}) during 50 cycles.

Figure 6 shows the cyclic voltammogram of the first five cycles for the $Li/LiNi_{1/2}Mn_{1/2}O_2$ cell between 2.5 and 4.6 V. The interesting feature is the difference in peak position between the first and subsequent cycles. The first anodic scan has two oxidation peaks, a major peak centered at 4.03 V and a minor one at 4.5 V corresponding to the irreversible capacity seen in the first charge curve. In the subsequent cycling, occurred only one major anodic and one major cathodic peak centered at 3.97 and 3.66 V, respectively. This is consistent with the results from the charge/discharge experiment shown in Figure 5(a), which shows only one charge and discharge plateau. Moreover, no reduction peak near 3.2 V was observed due to the reduction of Mn^{4+} to Mn^{3+}.

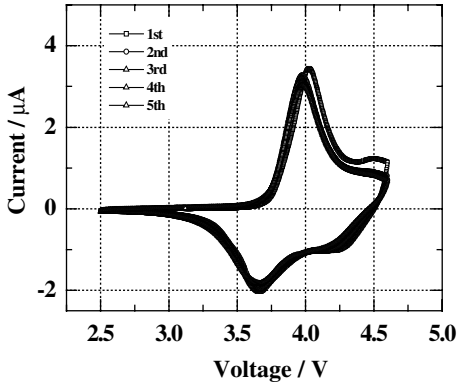

Fig. 6. Cyclic voltammetry profile of $Li/LiNi_{1/2}Mn_{1/2}O_2$ cell between 2.8 and 4.6 V.

In order to investigate the effect of electrochemical stability of the $LiNi_{1/2}Mn_{1/2}O_2$ materials at higher voltages, the upper cut-off voltages were changed to 4.4, 4.5 and 4.6 V and the results are shown in Figure 7. The cathodes were first galvanostatically charged and subsequently discharged by applying a current density of 20 mA g^{-1} at 30 °C. It was observed that raising the upper cut-off voltage limit does not change the voltage profiles irrespective of some increase in Internal Resistance (IR). The discharge capacities increase gradually with increase in the upper cut-off voltage limit. The $LiNi_{1/2}Mn_{1/2}O_2$ electrode delivers initial discharge capacities of 152, 163, 183, and 189 mA h g^{-1} in the voltage range 2.8–4.3, 2.8–4.4, 2.8–4.5, and 2.8–4.6 V, respectively, with good cyclability

Figure 8(a) shows the discharge curves for the pristine and $Al(OH)_3$-coated $LiNi_{1/2}Mn_{1/2}O_2$ electrodes as a function of current density (20–320 mA g^{-1}) between

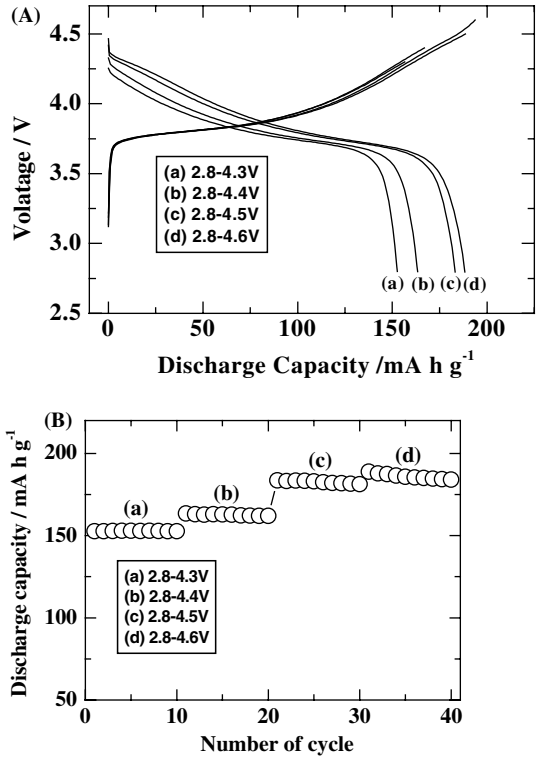

Fig. 7. (A) Voltage curves of $Li/LiNi_{1/2}Mn_{1/2}O_2$ cell changing upper cut-off voltage limit and (B) Specific discharge capacity of $Li/LiNi_{1/2}Mn_{1/2}O_2$ cell as a function of cycle number.

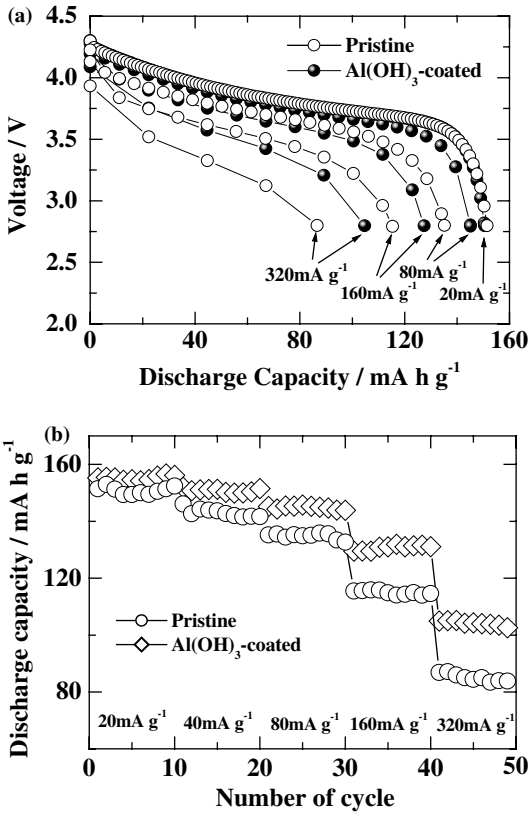

Fig. 8. (a) Cycling charge/discharge curves and (b) variation of specific discharge capacity as a function of current density for the pristine and $Al(OH)_3$-coated $Li/LiNi_{1/2}Co_{1/2}O_2$ cell between 2.8 and 4.4 V at 55 °C.

2.8 and 4.3 V at 55 °C. The corresponding discharge capacities vs cycle number are shown in Figure 8(b). The cells were charged using a current density of 20 mA g^{-1} before each discharge test. The discharge capacities of two electrodes at lower current density (20 mA g^{-1}) are identical (152 mA h g^{-1}), but the capacity retention and discharge capacity at higher current densities are significantly different. Apparently, the discharge voltage profile as well as specific discharge capacity of the $Al(OH)_3$-coated $LiNi_{1/2}Mn_{1/2}O_2$ electrode is much higher than the discharge voltage profile and specific discharge capacity of the pristine electrode at higher current densities. The $Al(OH)_3$-coated electrode clearly has a higher rate capability than the pristine electrode. The pristine $LiNi_{1/2}Mn_{1/2}O_2$ electrode had a capacity of 152, 135, and 87 mA h g^{-1} at 20 (0.1 C), 80 (0.5 C), and 320 (2 C) mA g^{-1}, respectively, while the discharge capacities of the $Al(OH)_3$-coated electrode were 155, 146, and 105 mA h g^{-1} at the corresponding current density. The capacity retention of the $Al(OH)_3$-coated $LiNi_{1/2}Mn_{1/2}O_2$ electrode at 320 mA g^{-1} is about 68% of its initial capacity at 20 mA g^{-1} while that of pristine electrode delivered only 57% at the same current density. The cycling behavior and rate capability of the $Al(OH)_3$-coated $LiNi_{1/2}Mn_{1/2}O_2$ electrode clearly shows the impact of $Al(OH)_3$ coating in protecting the surface of the $LiNi_{1/2}Mn_{1/2}O_2$ particle.

To examine the surface changes for the pristine and $Al(OH)_3$-coated $LiNi_{1/2}Mn_{1/2}O_2$ electrodes, AC

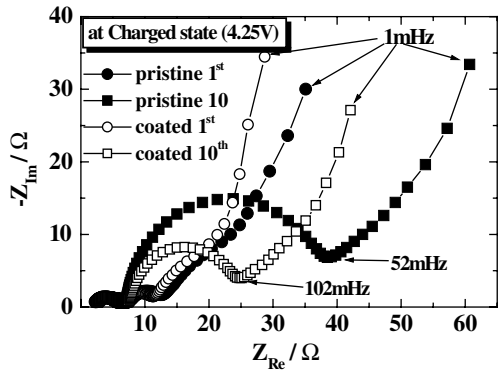

Fig. 9 Impedance spectra at charged state (4.25 V) of $Li/LiNi_{1/2}Mn_{1/2}O_2$ electrode (pristine and $Al(OH)_3$-coated) after 1st and 10th cycle.

impedance was measured on both electrodes. Both electrodes initially cycled once. Figure 9 illustrates the impedance spectra at charged state (4.25 V) of both electrodes after 1 and 10 cycles. The impedance spectra consist of two semicircles in the high- and intermediate-frequency ranges and a line inclined at constant angle to the real axis in the low-frequency range. The two semicircles in the higher and intermediate frequency range might be due to the contact resistance at the composite cathode and the charge transfer reaction at the interface of the cathode/electrolyte [17]. Although the first semicircle for the pristine and $Al(OH)_3$-coated $LiNi_{1/2}Mn_{1/2}O_2$ electrodes during the 1st and 10th cycles is very similar, considerable difference for the second semicircle between the pristine and $Al(OH)_3$-coated $LiNi_{1/2}Mn_{1/2}O_2$ electrode on 10th cycling is observed. The second semicircles were enlarged for both electrodes after 10 cycles but the second semicircle for the $Al(OH)_3$-coated is much smaller than that of pristine $LiNi_{1/2}Mn_{1/2}O_2$ electrode. The large decrease in charge transfer resistance may be attributed to the suppression of surface reactions between the cathode surface and electrolyte by coating of $Al(OH)_3$.

Recently, we reported that ZnO coated on $LiNi_{0.5}Mn_{1.5}O_4$ particles played an important role as an HF-getter and the ZnO-coated $LiNi_{0.5}Mn_{1.5}O_4$ showed significantly better cycling behavior and structural stability during cycling at 5 V range (3.5–5.2 V) and 55 °C than pristine $LiNi_{0.5}Mn_{1.5}O_4$ [11, 18]. Considering that Al is an amphoteric element similar to Zn, we presume that $Al(OH)_3$ on the particle surface reacted with HF to form Al–F compounds (e.g., $AlF_3 \cdot 3H_2O$), as suggested by Zheng et al. [19] and Kim et al. [20], and suppressed the dissolution of cations into the electrolyte. Further studies are needed to clearly understand the improvement in electrochemical performance for $Al(OH)_3$-coated $LiNi_{1/2}Mn_{1/2}O_2$ electrodes.

4. Conclusion

Spherical $LiNi_{1/2}Mn_{1/2}O_2$ powders with high specific capacity and tap density were synthesized by

coprecipitation. The measured tap-density of the prepared $LiNi_{1/2}Mn_{1/2}O_2$ powders was as high as 2.2 g cm^{-3}. In the voltage ranges 2.8–4.3, 2.8–4.4, 2.8–4.5, and 2.8–4.6 V, the specific gravimetric discharge capacities of the $Li[Ni_{1/2}Mn_{1/2}]O_2$ electrode were 152, 163, 183, and 189 mA h g^{-1}, respectively, with excellent cyclability with 20 mA g^{-1} of current density at 30 °C. The charge/discharge and cyclic voltammogram of the $Li/LiNi_{1/2}Mn_{1/2}O_2$ cell showed only one redox peak and no reduction peak near 3.2 V due to the reduction of Mn^{4+} to Mn^{3+}, implying that no significant structural change occurred during electrochemical cycling. $Al(OH)_3$-coated $LiNi_{1/2}Mn_{1/2}O_2$ showed excellent rate capability and cyclability at elevated temperature compared to the pristine electrode.

Acknowledgements

This research was supported by a University IT Research Center Project and by the part financial support of the Center for Nanostructured Materials Technology under '21st Century Frontier R&D Programs' of the Ministry of Science and Technology.

References

1. E. Rossen, C.D.W. Jones and J.R. Dahn, *Solid State Ionics* **57** (1992) 311.
2. M.E. Spahr, P. Novak, B. Schnyder, O. Hass and R. Nesper, *J. Electrochem. Soc.* **145** (1998) 1113.
3. T. Ohzuku and Y. Makimura, *Chem. Lett.* (2001) 744.
4. Z. Lu, D.D. MacNeil and J.R. Dahn, *Electrochem. Solid-State Lett.* **4** (2001) A191.
5. Y. Arachi, H. Kobayashi, S. Emura, Y. Nakata, M. Tanaka and T. Asai, *Chem. Lett.* **32** (2003) 60.
6. W.S. Yoon, Y. Paik, M. Balasubramanian, J. McBreen and C.P. Grey, *Electrochem. Solid-State Lett.* **5** (2002) A262.
7. J.S. Kim, C.S. Johnson and M.M. Thackeray, *Electrochem. Commun.* **4** (2002) 205.
8. S.H. Kang, J. Kim, Me.E. Stoll, D. Abraham, Y.-K. Sun and K. Amine, *J. Power Sources* **112** (2002) 41.
9. S.H. Park, S.W. Oh, S.G. Kang, S.T. Myung and Y.K. Sun, *Chem. Lett.* **33** (2004) 2.
10. S. Jouanneau, K.W. Eberman, L.J. Krause and J.R. Dahn, *J. Electrochem. Soc.* **150** (2003) A1637.
11. Y.-K. Sun, Y.-S. Lee, M. Yoshio and K. Amine, *Electrochem. Solid-State Lett.* **5** (2002) A99.
12. J. Cho, Y.J. Kim and B. Park, *Chem. Mater.* **12** (2000) 3788.
13. A. Chobelt, H.C. Shiao, H.-P. Lin, M. Salomon and V. Manivannan, *Electrochem. Solid-State Lett.* **4** (2001) A65.
14. Joint Committee on Powder Diffraction Standards, File no. 14-0117.
15. J. Ying, C. Wan, C. Jiang and Y. Li, *J. Power Sources* **99** (2001) 78.
16. T.Roisnel and J. Rodriguez-Carjaval, Fullprof Manual, Institut Laue-Langevin, Grnoble (2000).
17. Y.-K. Sun and S.-H. Jin, *J. Mater. Chem.* **8** (1998) 2399.
18. Y.K. Sun, K.J. Hong, Jai Prakash and K. Amine, *Electrochem. Commun.* **4** (2002) 344.
19. Z. Zheng, Z. Tang, Z. Zhang, W. Shen and Y. Lin, *Solid State Ionics* **148** (2002) 317.
20. J.-S. Kim, C.S. Johnson, J.T. Vaughey, S.A. Hackney, K.A. Walz, W.A. Zeltner, M.Z. Anderson and M.M. Thackeray, *J. Electrochem. Soc.* (in press).